Pergamon

PII: S0307-9322(96)00086-9

Int. J. Multiphase Flow Vol. 23, No. 4, pp. 631–650, 1997

Printed in Great Britain
0301-9322/97 $17.00 + 0.00

AN ANALYSIS OF THE DISTORTION AND BREAKUP MECHANISMS OF HIGH SPEED LIQUID DROPS

Z. LIU and R. D. REITZ

Engine Research Center, University of Wisconsin–Madison, Madison, WI 53706, U.S.A.

(Received 12 January 1996; in revised form 24 November 1996)

Abstract—A study was performed of the distortion and breakup mechanisms of liquid drops injected into a transverse high velocity air jet at room temperature and atmospheric pressure. The investigation included the use of ultra-high magnification, short-exposure photography to study the three drop breakup regimes previously referred to as the bag breakup regime, the shear or boundary-layer stripping breakup regime, and the 'catastrophic' breakup regime. In the experiments the initial diameters of the injected diesel fuel drops were 69, 121 and 198 μm, and the transverse air jet velocity was varied from 68 to 331 m/s. The experimental conditions correspond to drop initial Weber numbers of 56, 260 and 463 for the three breakup regimes. The drop Reynolds numbers (based on gas properties) ranged from 509 to 2488. It was found that the drop breakup process occurs in two stages. During the first stage, under the action of aerodynamic pressure, the drop distorts from its undisturbed spherical shape and becomes flattened, or disk shaped, normal to the air flow direction. This feature exists in all three drop breakup regimes. A dynamic drag model that is a modified version of the DDB (Dynamic Drag and Breakup) model and accounts for the increase of both the drop's frontal area and its drag coefficient as a function of its distortion was used to analyze the drop trajectory and its distortion during the first stage of the drop breakup process. During the second stage of the drop breakup process, the three drop breakup regimes display different breakup features. In the bag breakup regime the appearance and growth of holes on the bag sheet blown out of the center of the flattened drop is the dominant reason for the breakup; in the so-called shear or boundary-layer stripping breakup regime the results indicate that bending of the flattened drop's edge under the action of aerodynamic pressure, followed by production of folds on the bent sheet results in production of ligaments aligned in the direction of the air flow; and in the 'catastrophic' breakup regime the growth of capillary waves on the flattened drop surfaces, combined with the bending and folding of the sheet edge makes the breakup process demonstrate 'catastrophic' breakup characteristics. In addition, the experimental results confirm that for drops with different sizes, the same breakup regimes appear when the Weber number is held constant, and the Reynolds number does not play a dominant role. These results thus cast considerable doubt on the validity of the widely used 'shear' or 'boundary-layer stripping' drop breakup theories in which viscous effects would be important.

Key Words: liquid drop, drop distortion, drop trajectory, drop breakup

1. INTRODUCTION

It is well known that the combustion efficiency in diesel engines, gas turbine engines, and oil burners is influenced by the rate of vaporization of the liquid fuel which is strongly dependent on the liquid fuel atomization process. The atomization can be enhanced by increasing the relative velocity between the liquid fuel and the ambient gas, as described by Chigier and Reitz (1996), Lefebvre (1989), and Hwang *et al.* (1996). The fundamental mechanisms of atomization have been under extensive experimental and theoretical study for many years. Reviews of liquid atomization mechanisms have been provided by Reitz and Bracco (1986), Krzeczkowski (1980), Pilch and Erdman (1987), Hsiang and Faeth (1992), and Wu and Faeth (1993).

Studies of single liquid drop breakup mechanisms are of interest since they form the foundation of the study of atomization. So far, numerous studies on liquid drop breakup have been conducted, but most progress in understanding the breakup process has only been made for the breakup of relatively low speed drops. As the relative velocity between the drop and gas increases, three basic regimes of drop breakup are encountered which have been referred to as the bag breakup regime (Kennedy and Roberts 1990), the 'shear' or 'boundary layer stripping' breakup regime (Ranger and Nicholls 1969), and the catastrophic breakup regime (Reinecke and Waldman 1970).

Some criteria for predicting drop breakup regime transitions in steady high-speed gas flows have been presented by Krzeczkowski (1980), Wu *et al.* (1993) and others. The Weber number, $We = \rho_G U^2 d/\sigma$ (where ρ_G is the gas density, U is the relative velocity between the drop and the gas, d is the drop diameter and σ is the surface tension), and the Ohnesorge number, $Z = \mu_L/(\rho_L d\sigma)^{1/2}$ (where μ_L is the liquid viscosity, and ρ_L is the liquid density) have been found to be important parameters. For example, for Ohnesorge numbers less than one ($Z < 1$, i.e. all but the most viscous fluids) significant drop distortion and oscillation is noticed starting at $We \sim 1$ (the Weber number is based on the undisturbed drop diameter). Bag breakup commences at about $We = 12$. Transition to 'shear-type' breakup occurs at higher Weber numbers ($We > 80$) and 'multimode' breakup (combined bag- and shear-type) occurs in the intermediate Weber number range (Wu *et al.* 1993). For high viscosity liquids, Wierzba and Takayama (1988), and Wu *et al.* (1993) concluded that the Ohnesorge number must be introduced and the breakup regime transitions are moved to higher Weber numbers.

There are at least two different popular theories that explain the mechanism of the 'shear-type' or 'boundary layer stripping-type' breakup, as reviewed for example by Wierzba and Takayama (1988). The first, developed by Ranger and Nicolls (1969) and others, attributes the breakup to a boundary layer separation process. Shearing action exerted by the high speed gas flow on the drop periphery causes the formation of a boundary layer at the surface of the liquid. In the Ranger and Nicolls' model it is assumed that the thickness of this layer controls the rate at which liquid leaves (i.e. is stripped from) the surface of the drop at its equator. A key element of this theory is that the breakup is driven by the gas shear at the liquid interface, and therefore the drop Reynolds number based on the gas properties enters the model formulation. A second theory, proposed by Hinze (1955), Engel (1958) and others, attributes the breakup to the formation and breaking of (capillary) surface waves formed on the windward surface of the drop. Several detailed models of drop breakup based on these models have also been proposed, such as that of Collins and Charwat (1971).

With these conflicting theories, it can be concluded that there is still much uncertainty about the breakup mechanisms of high speed drops. In fact, it is the breakup of high speed drops that is of the most interest in many practical applications. As the air velocity increases, aerodynamic and possibly viscous effects become more important and the process becomes more difficult to analyze. A detailed insight into fundamental mechanisms which control the breakup of high speed liquid drops has not been arrived at, partly because clear experimental evidence for the breakup mechanisms is lacking, and thus models of disintegration mechanisms are still only speculative (e.g. Hwang *et al.* 1996 and Wu *et al.* 1993).

The objective of the present work was to investigate the breakup mechanisms of liquid drops injected into a transverse high velocity air flow at room temperature and atmospheric pressure conditions. Drops with different sizes were used to give drop Weber numbers selected to produce breakup in the bag, shear, and catastrophic breakup regimes. Based on the information presented by the experimental results, the breakup mechanisms of liquid drops in the three breakup regimes are analyzed in detail.

2. EXPERIMENTS

The experimental apparatus consists of a liquid drop generator and an air nozzle with a converging exit, which are arranged in a cross flow pattern, as shown in figure 1. A monodisperse stream of liquid drops is injected horizontally into the air jet from right to left, and the air flows vertically from top to bottom. The monodisperse liquid drop stream is generated by using a drop generator developed by Berglund and Liu (1973). The drop size is determined from the following equation

$$d = \left(\frac{6Q}{\pi f}\right)^{1/3} \qquad [1]$$

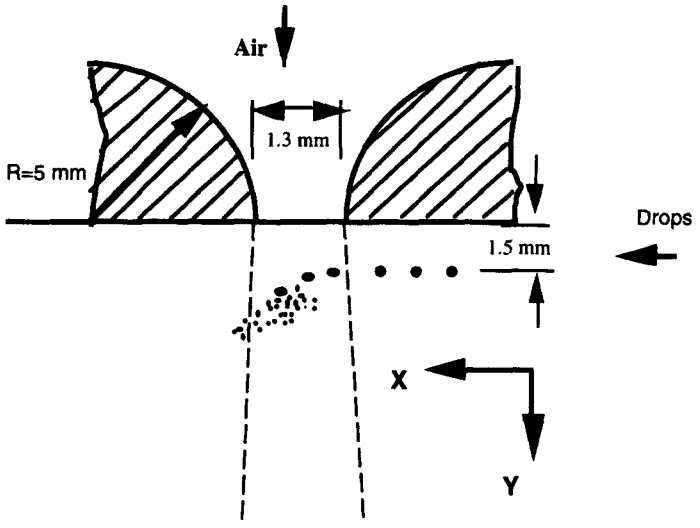

Figure 1. Schematic diagram of experimental apparatus.

where Q is the volumetric flow rate and f is the applied frequency. The optimum frequency is obtained from the Rayleigh wave length for the most unstable disturbance, *viz.*

$$f_{\text{Rayleigh}} = \frac{V_j}{\lambda_{\text{optimum}}} = 0.282 \frac{Q}{D_j^3} \quad [2]$$

where D_j is the injector orifice diameter, V_j is the liquid jet velocity and λ_{optimum} is the wave length of the most unstable disturbance. In this study the initial diameters of the injected diesel fuel drops are 69, 121 and 198 μm, which correspond to the use of fuel nozzle orifice diameters of 28, 54 and 99 μm, and applied frequencies of 86, 50 and 27 kHz, respectively. The piezo-electric drop generator is operated using a square wave signal with a peak-to-peak voltage of 20 V. Under these conditions, for the fuel nozzle with the orifice diameter of 28 μm, the drops are injected at a (horizontal) velocity of 23.8 m/s; for the fuel nozzle with the orifice diameter of 54 μm, the drops are injected at a velocity of 19.8 m/s; and for the fuel nozzle with the orifice diameter of 99 μm, the drops are injected at a velocity of 14.3 m/s. The fuel used is Benz oil UCF-1 test fuel which meets SAE J967d, ISO 4113 (a diesel-type fuel). The viscosity is 0.00217 Ns/m^2, the density is 824 kg/m^3, the surface tension is 0.02 kg/s^2, the flash point is 348 K, and the t-90 distillation point is 483 K.

The air nozzle exit is a rectangular slit with $h = 1.3$ mm and $b = 10$ mm, where h is the slit width and b is the slit length (i.e. into the plane of the paper in figure 1). The 5 mm long air nozzle passage features a rounded entrance with radius $R = 5$ mm (i.e. $R/b = 0.5$), to ensure that the velocity profile at the nozzle exit is flat so that boundary layer effects could be minimized. The rapid contraction produces a well characterized laminar flow at the nozzle exit plane, as confirmed by Liu and Reitz (1993) by means of LDV velocity measurements. When the distance between the injecting drop stream and the nozzle exit is decreased, the shear layer thickness at the point of entry of the drops into the jet will be reduced, which also decreases the boundary layer effects. In the present experiments the distance of 1.5 mm is selected, and the shear edge thickness is estimated to be 158 μm. The time for the injected drops to traverse the shear layer and enter the air jet thus ranges between 6.6 and 11 μs depending on the drop's injection velocity.

Figure 2 shows the optical system used in experiments which consists of an Xenon high intensity nano-pulse light source and a Nikon 35 mm camera equipped with a Questar QM-100 long distance microscope. The nano-pulse light source is a Xenon Model N789B with a pulse duration of 20 ns. High sensitivity Kodak T-Max 400 film is used for the photography. The magnification was $\times 15$ on the film negatives. Considerations of the diffraction limit of the lens system used lead to the estimate that dimensions can be resolved in the photographs down to about 3 μm (Liu and Reitz 1993).

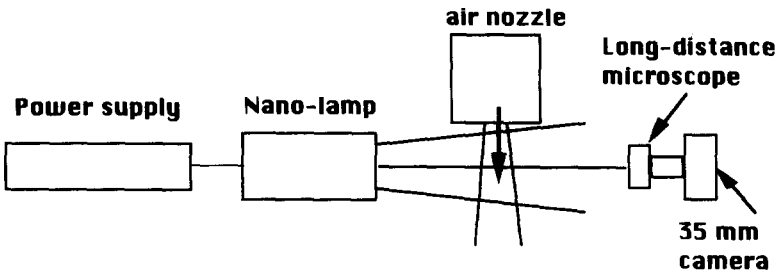

Figure 2. Schematic diagram of optical arrangement.

The breakup regimes are classified into three basic types of regimes which are called the bag, shear or boundary layer stripping and 'catastrophic' regimes (Liu and Reitz 1993). Three air flow velocities were selected to give breakup in the three breakup regimes: 68 m/s (bag), 147 m/s (shear), 196 m/s (catastrophic) for the drops with injected diameters of 198 μm. For the smaller injected drop tests the air jet velocities are adjusted such that the Weber numbers were the same as for the large drop tests, that is, for the bag breakup regime the Weber number was We = 56, for the shear breakup regime the Weber number was We = 260, and for the catastrophic breakup regime the Weber number was We = 463. The operating variables of each case are summarized in table 1. Table 1 also includes the drop Reynolds number based on the gas properties, $\mathrm{Re}_G = \rho_G U d/\mu_G$, which is relevant for considerations of boundary layer shear flows.

3. DROP DISTORTION

Experiments clearly show that when a liquid drop is exposed to a high velocity gas flow, it distorts and breaks up. To predict the distortion and the breakup, several mathematical models have been proposed, for example, the TAB model (O'Rourke and Amsden 1987) and the DDB model (Ibrahim *et al.* 1993).

Ibrahim *et al.* (1993) proposed the DDB (Drop Deformation and Breakup) model, which is based on the drop dynamics in terms of the motion of the center of mass of the half-drop. It is assumed that the liquid drop is deformed due to a pure extensional flow from an initial spherical shape of radius, r, into an oblate spheroid of an ellipsoidal cross section with major semiaxis, a, and minor semiaxis, b. The internal energy of the half-drop comes from its kinetic and potential energies

$$\frac{\mathrm{d}E}{\mathrm{d}t} = \frac{2}{3}\pi r^3 \rho_L \frac{\mathrm{d}y}{\mathrm{d}t}\frac{\mathrm{d}^2 y}{\mathrm{d}t^2} + \frac{9\pi^2\sigma}{8} y\left[1 - 2\left(\frac{cy}{r}\right)^{-6}\right]\frac{\mathrm{d}y}{\mathrm{d}t} \qquad [3]$$

where $c = 3\pi/4$, y is the distance from the center of mass of the deforming half-drop to its pole, as shown in figure 3, and this is equal to the work done by pressure and viscous forces, which can

Table 1. Experimental conditions and variables

Case	Figure	Air velocity (m/s)	Drop size (μm)	Weber number	Reynolds number	Drop horizontal velocity (m/s)
1	4	68	198	56	863	14.3
2	5	147	198	260	1866	14.3
3	6	196	198	463	2488	14.3
4	7	87	121	56	675	19.8
5	9	188	121	260	1458	19.8
6	11	250	121	463	1939	19.8
7	8	115	69	56	509	23.8
8	10	248	69	260	1097	23.8
9	12	331	69	463	1464	23.8

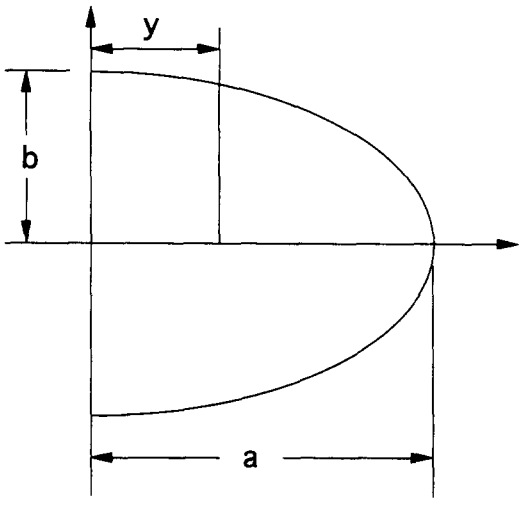

Figure 3. The deforming half-drop diagram.

be written as

$$\frac{dW}{dt} = -\frac{\pi}{4} r^2 \rho_G U^2 \frac{dy}{dt} + \frac{8}{3} \pi r^3 \mu_L \left(\frac{1}{y}\frac{dy}{dt}\right)^2. \quad [4]$$

Letting $y_1 = y/r$ and $t_1 = tU/r$ to nondimensionalize [3] and [4] gives (Ibrahim *et al.* 1993)

$$\frac{d^2 y_1}{dt_1^2} = \frac{3}{8K} - \frac{27\pi^2}{8K\mathrm{We}} y_1[1 - 2(cy_1)^{-6}] - \frac{8N}{K\mathrm{Re}} \frac{1}{y_1^2}\frac{dy_1}{dt_1} \quad [5]$$

where $K = \rho_L/\rho_G$, $\mathrm{We} = \rho_G U^2 d/\sigma$, $\mathrm{Re} = \rho_G U d/\mu_G$ and $N = \mu_L/\mu_G$. By solving [5], the major and minor semiaxes can be obtained from $a = 3\pi y/4$ and $b = r^3/a^2$.

4. DROP TRAJECTORY

The distortion of the drop has an important effect on its drag coefficient, and hence its trajectory (Liu and Reitz 1993). The drop's acceleration is obtained from its equation of motion

$$\rho_L V_d \frac{d\mathbf{u}}{dt} = C_D A_f \frac{\rho_G U^2}{2} \{\mathbf{U}/|\mathbf{U}|\} \quad [6]$$

where $\mathbf{u}$ is the drop velocity vector, $\mathbf{U}$ is the drop-gas relative velocity vector, ρ_L is the liquid density, ρ_G is the gas density, $V_d = 4\pi r^3/3$ and $A_f = \pi r^2$ are the volume and frontal area, respectively (for a spherical drop), C_D is the drop drag coefficient. In most spray modeling applications, the drop Reynolds numbers are high enough that corrections to the Stokes drag law are also required. The drop drag coefficient is specified as a function of the drop Reynolds number using solid-sphere correlations (Liu *et al.* 1993)

$$C_{D,S} = \frac{24}{\mathrm{Re}}\left(1 + \frac{1}{6}\mathrm{Re}^{2/3}\right) \quad \mathrm{Re} \leqslant 1000 \quad [7a]$$

$$C_{D,S} = 0.424 \quad \mathrm{Re} > 1000. \quad [7b]$$

The effects of drop oscillation and distortion on the drop drag coefficient have been considered by Liu and Reitz (1993) and Liu *et al.* (1993) who used the TAB model to estimate the distortion of the drops. The drop drag coefficient was assumed to be related to the magnitude of the drop deformation with

$$C_D = C_{D,S}(1 + 2.632y'). \quad [8]$$

Equation [8] expresses the fact that the drag coefficient of a distorting drop should lie between that of a rigid sphere and that of a disk, whose drag coefficient at high Reynolds numbers is about 3.6 times higher than that of a sphere. Therefore, the drag coefficient in [8] was calculated using

$$y' = \min\left(1, \left\{\frac{a}{r} - 1\right\}\right) \quad [9]$$

such that the drag coefficients of a spherical drop and a disk were also recovered in the undistorted and fully distorted drop limits, respectively. The drop is assumed to be fully distorted when $a = 2r$ (Ibrahim *et al.* 1993).

In the present study it was found that the TAB drop drag model used by Liu and Reitz (1993) and Liu *et al.* (1993) significantly underestimated drop drag effects for high speed drops. As noted in figure 3, the drops undergo significant flattening due to the dynamic pressure effect as soon as they enter the air jet. This changes the frontal area of the drop exposed to the flow. The flattening occurs prior to significant mass loss from the drops due to breakup. To account for the effect of distortion, the DDB model was used in the present study to compute the drop frontal area. In this case

$$A_f = \pi a^2. \quad [10]$$

5. RESULTS AND DISCUSSION

By using the experimental apparatus shown in figure 1, and the optical system shown in figure 2, high-magnification, ultra-short duration pulse-illumination photographs were taken of the breakup processes of drops with three different initial sizes to reveal drop breakup mechanisms under typical bag, so-called shear or boundary-layer stripping, and 'catastrophic' breakup regime conditions. From inspections of the experimental results, it was found that the breakup processes of the liquid drops could be classified roughly into two stages. During the first stage of the drop breakup process, the drops experience a shape change, and drops operating in all three drop breakup regimes share this common feature. During the second stage of the drop breakup process, the shape-changed drops undergo a disintegration, and the three drop breakup regimes display different breakup mechanisms. These two stages of drop breakup are first described in the following sections, and then the drop distortion process itself is further analyzed to quantify its effect on drop drag and drop trajectories.

5.1. First breakup stage

When a spherical liquid drop is exposed to a steady air stream, the drop is influenced by the variation in the distribution of air pressure around the drop. Under equilibrium conditions the internal pressure at any point on the drop surface is just sufficient to balance the external aerodynamic pressure and the surface tension pressure. However, when a steady air stream flows around a drop, the air velocity distribution and the air pressure distribution at any point on the drop surface are not uniform. The air velocity has a maximum at the equator of the drop, and equals zero at the drop's poles (the stagnation point). Thus, in accordance with Bernoulli's law the air pressure becomes higher at the poles, and lower at the equator. In this situation the external aerodynamic pressure causes the drop to distort from its undisturbed spherical shape and to become flattened to form an oblate ellipsoid, normal to the air flow direction. As the velocity at the equator of drop increases, the Bernoulli pressure difference increases accordingly, which leads to further flattening of the drop, and finally the drop becomes disk shaped. This process is clearly seen in the photographs of figures 4–12. In the figures the stream of monodisperse injected drops enters at the top right of each photograph, as indicated in figure 1. The experimental conditions for each case are summarized in table 1.

From inspection of all the experimental results shown in figures 4–12, it can be seen that this flattening process occurs as soon as the injected drops enter the air jet in all drop breakup regimes. As the drop deforms, its surface curvature at its equator continuously increases. This results in corresponding increases in surface tension forces that act against the Bernoulli pressure. Whether

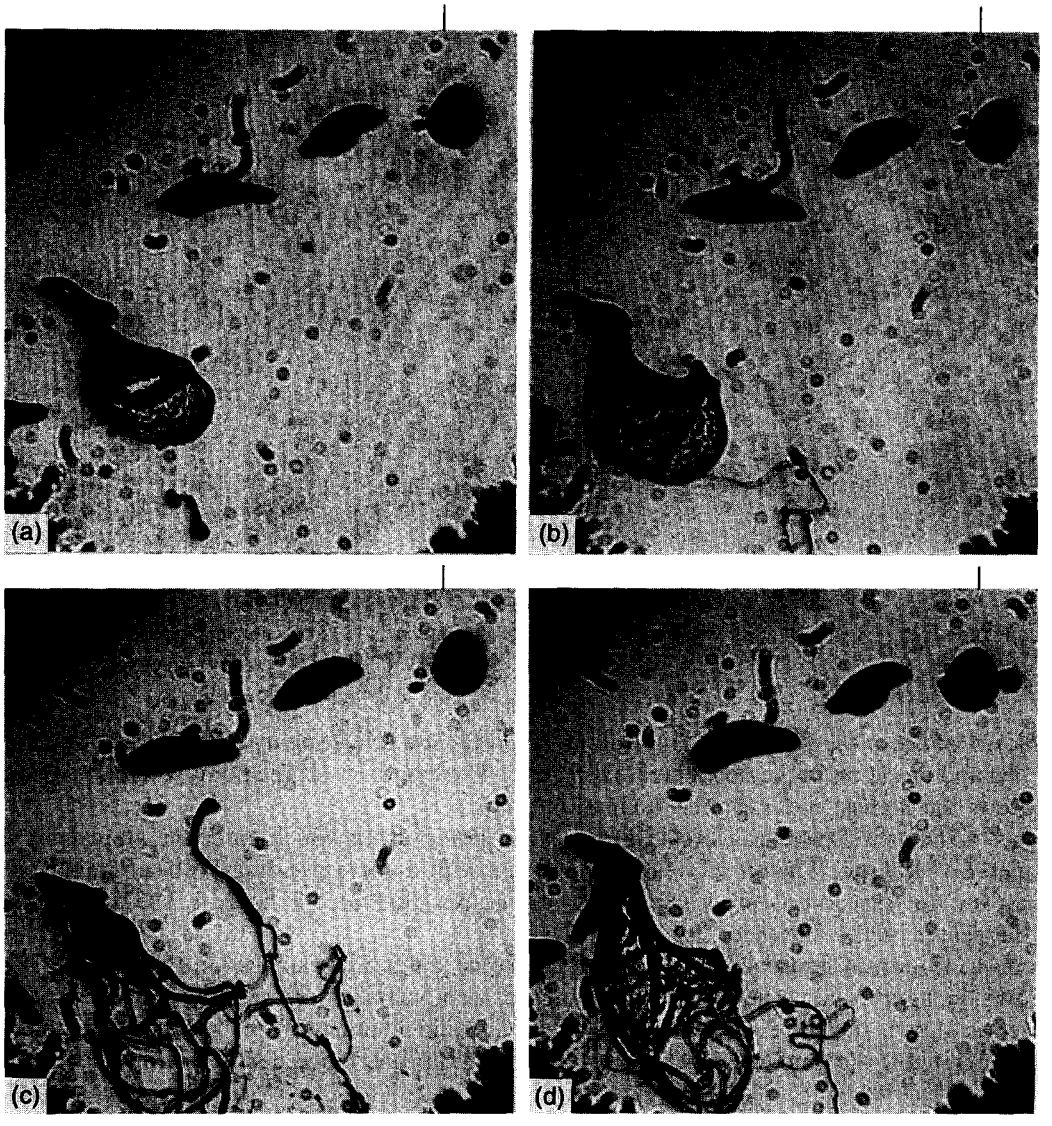

Figure 4. Photograph of bag breakup of drop with a diameter of 198 μm, under the action of an air jet velocity of 68 m/s with a corresponding Weber number of 56. Line at upper right indicates location of air jet edge.

or not the drop achieves an equilibrium shape depends on the relationship between the Bernoulli pressure and the surface tension pressure. Before the equilibrium is destroyed, the drop will continue to be deformed without disintegrating (Anilkumar *et al.* 1993; and Lee *et al.* 1991). Detailed analysis and modeling of the distortion of the drops and its effect on the drop drag is presented after the second stage of the breakup process is discussed next.

5.2. Second breakup stage

As the relative velocity increases, the bag, so-called shear or boundary-layer stripping, and 'catastrophic' breakup regimes are encountered, respectively, as shown in figures 4–12. Figures 4–6 show the breakup processes in the three regimes for the 198 μm diameter injected drops; the pairs of figures 7 and 8, 9 and 10, and 11 and 12 show breakup in the three breakup regimes with 121 and 69 mm diameter injected drops, respectively. During the second stage of the drop breakup process, the flattened drops in the three breakup regimes are found to exhibit different disintegration mechanisms, as follows.

5.2.1. Bag breakup. When the air stream velocity is relatively low, the bag breakup phenomenon appears. The accelerating drop becomes increasingly flattened, and at a critical relative velocity, the flattened drop becomes thin enough that it presents a concave surface near its pole and soon

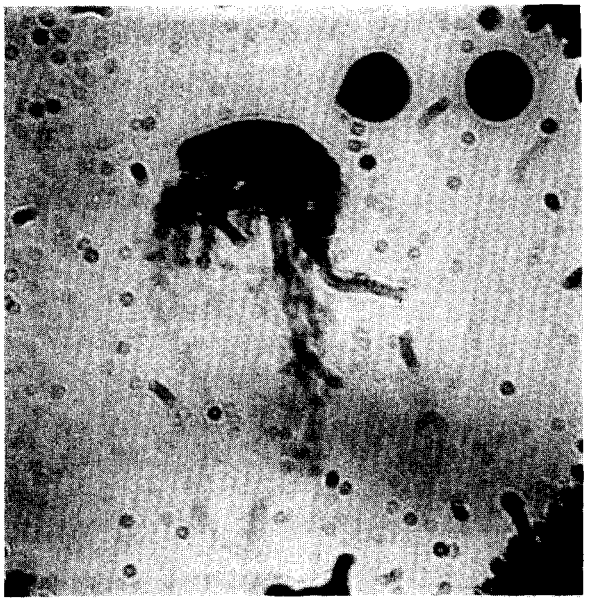

Figure 5. Photograph of shear breakup of drop with a diameter of 198 μm, under the action of an air jet velocity of 147 m/s with a corresponding Weber number of 260.

it is blown out into the form of a thin hollow bag attached to a roughly circular rim. The bag is stretched and swept off in the downstream direction. The bag forms at the point where the dynamic pressure is the highest, i.e. near the stagnation point.

Figure 4 shows a typical bag breakup process of liquid drops which enter the air stream with a diameter of 198 μm. The air jet velocity is 68 m/s with a corresponding Weber number of 56. The bag and the rim can be seen clearly in the photographs illustrated in figure 4. The bag originates near the center of the flattened disc.

From inspection of figure 4, it is observed that some small holes appear on the thin bag sheet, as shown in figure 4(a). Under the action of the aerodynamic pressure, these holes gradually enlarge, as shown in figure 4(b) and (c), and then liquid filaments form between the holes, as illustrated in figure 4(c) and (d), which causes the bag to rupture. Upon disintegration, the filaments

Figure 6. Photograph of catastrophic breakup of drop with a diameter of 198 μm, under the action of an air jet velocity of 196 m/s with a corresponding Weber number of 463.

Figure 7. Photograph of bag breakup of drop with a diameter of 121 μm, under the action of an air jet velocity of 87 m/s with a corresponding Weber number of 56.

produce very fine drops, while the rim, which contains most of the mass of the original drop, breaks up into larger drops a short time later.

The formation of the original holes in the stretched bag could be caused by disturbances in the air stream or due to the presence of particles in the liquid that serve as inception sites (Taylor 1959; Spielbauer and Aidum 1994). Because the sheet thickness of the bag is not uniform, some points are very thin where it is easy for small holes to form under the action of locally high aerodynamic pressures or other disturbances.

Figures 7 and 8 show experimental results of bag breakup of the smaller drops but with the air velocity adjusted such that the Weber number is also equal to 56. In figure 7, the original drop size is 121 μm, and the air velocity is 87 m/s. In figure 8, the original drop size is 69 μm, and the air velocity is 115 m/s. From inspection of figures 4, 7 and 8, it can be seen that all of them illustrate

Figure 8. Photograph of bag breakup of drop with a diameter of 69 μm, under the action of an air jet velocity of 115 m/s with a corresponding Weber number of 56.

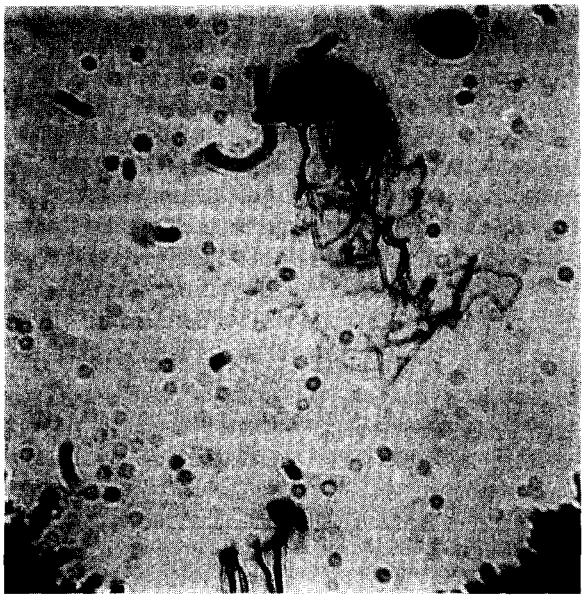

Figure 9. Photograph of shear breakup of drop with a diameter of 121 μm, under the action of an air jet velocity of 188 m/s with a corresponding Weber number of 260.

the typical bag breakup features. These results indicate that the Weber number is the appropriate scaling parameter for drop breakup in the bag breakup regime.

5.2.2. Shear or boundary-layer stripping breakup. As the air velocity is increased further, breakup now occurs at the equatorial edges of the flattened drop, which can be seen in figure 5, in which the original drop size is 198 μm, and the air velocity is 147 m/s with a corresponding Weber number of 260. The breakup process is distinctly different from that in the bag breakup regime. Instead of its pole region being blown out into a thin hollow bag anchored to its rim (the equator), the drop is deformed in the opposite direction and it presents a convex surface to the flow of air. The edges of the saucer-shaped drop are drawn out into a thin sheet by drag forces, and then the sheet is split up into fine filaments or ligaments, which later break up into small drops.

Figure 10. Photograph of shear breakup of drop with a diameter of 69 μm, under the action of an air jet velocity of 248 m/s with a corresponding Weber number of 260.

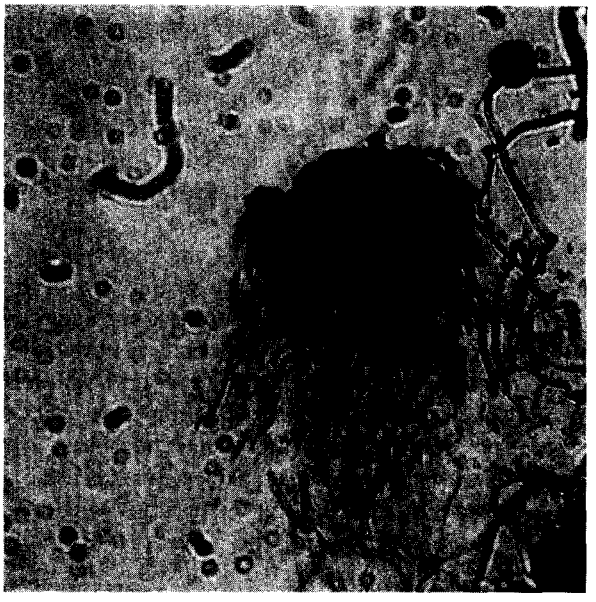

Figure 11. Photograph of catastrophic breakup of drop with a diameter of 121 μm, under the action of an air jet velocity of 250 m/s with a corresponding Weber number of 463.

Because the velocity at the equator of the drop is very high, a suction stress toward the outside of the drop occurs in the horizontal direction, which leads to the horizontal extension of the drop. From mass conservation, the thickness of the flattened drop will decrease from its center to the edge, and the edge will be very thin, and thus it tends to follow the air flow direction, due to its low inertia. Note that this sheet-thinning breakup mechanism is fundamentally different from the two previously proposed breakup mechanisms of Ranger and Nicolls (1969) and Hinze (1955), mentioned earlier. Those theories attribute the mass loss process that occurs at drop's equator to boundary layer stripping or to surface wave breaking processes, respectively, and those hypothetical breakup mechanisms would apply even to a spherical (i.e. undistorted) drop. Instead, the present photographs reveal that breakup actually originates from the flattened sheet at the edge of the drop that is deflected by the airflow.

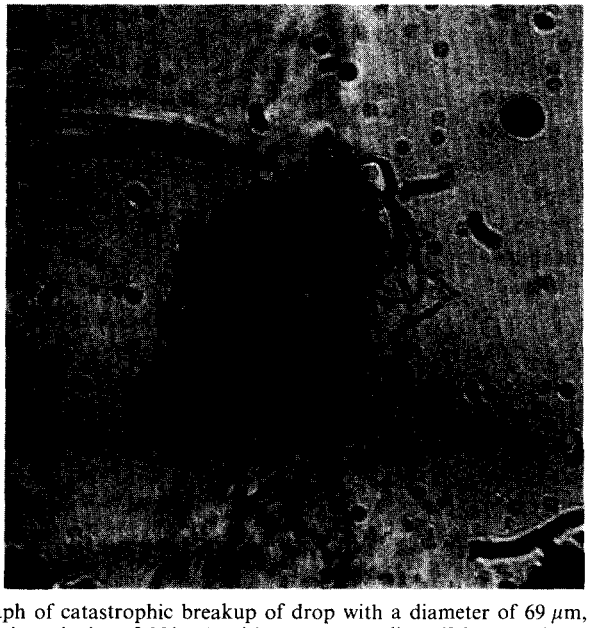

Figure 12. Photograph of catastrophic breakup of drop with a diameter of 69 μm, under the action of an air jet velocity of 331 m/s with a corresponding Weber number of 463.

Considerable work has been done by Anilkumar *et al.* (1993), Lee *et al.* (1991) and Danilov and Mironov (1992) dealing with the breakup of drops in high intensity sound fields. In these levitating drop experiments the drop is always fixed spatially during the flattening process, making the study of breakup easier. These works are of interest to the present study because the acoustic pressure is analogous to the dynamic pressure effect in steady flows, as concluded by Danilov and Mironov (1992). Under the action of an intense sound field the flattened drop also deforms into a knife-edged disc structure.

In the situation of present experiments, it appears that the very thin edge sheet of the flattened drop, which has a low inertia, is deflected in the direction of the flow of air by the blowing of the air stream. This causes the flattened drop to present a convex surface facing the air stream. The breakup of the deflected sheet then evidently occurs by a mechanism that is similar to the 'stretched streamwise ligament breakup' mechanism described by Stapper and Samuelsen (1990). Stapper and Samuelsen found that flat liquid sheets exposed to coflowing gases with high relative velocities exhibit cellular breakup patterns where thin liquid membranes are formed between growing streamwise and spanwise vortical waves on the sheet surface. In the case of high gas velocities, the streamwise waves dominated and led to the formation of streamwise ligaments, which are also seen in the breakup of the sheet formed at the edge of the drops in the present study.

As the circular flattened edge of the drop is deflected in the direction of the air flow, the distance from its center to its edge periphery is reduced. Under this condition it also follows from mass conservation arguments that the production of folds on the sheet edge in the azimuthal direction is inevitable (e.g. consider a sheet of paper that is crumpled around a ball). In this case, the folding of the thin edged-sheet results in the production of the filaments that are seen in the photographs to be aligned with the flow of air.

Note that conventional wave stability theories for the breakup of thin liquid sheets predict that the breakup results in spanwise ligaments that are oriented transversely to the flow direction (Squire 1953), in disagreement with the present photographic evidence. Indeed, Stapper and Samuelsen also noted that the spanwise breakup mode was dominant only at low gas co-flow velocities on their flat liquid sheets. In the present study the thin sheet edge is bent in the direction of the high speed air flow, and it is reasonable that the ligaments produced would be aligned in the direction of the flow of air, as in Stapper and Samuelsen's (1990) high relative velocity experiments. Once the ligaments are formed, their mechanism of breakup is likely to be similar to that of jet breakup; namely, Rayleigh capillary wave pinching which has been studied extensively both experimentally and theoretically (e.g. Reitz and Bracco 1986).

In the boundary layer stripping model it is assumed that viscous shear forces in the air and liquid boundary layers are responsible for the liquid that is 'stripped' from the drop's equator. The present interpretation is quite different since the drop flattening and breakup mechanism described above would still apply even in an inviscid liquid and gas flow.

In the boundary layer stripping model it is presumed that viscous shear forces are dominant, and thus the breakup process should scale with the Reynolds number, since the Reynolds number is a ratio of inertia to viscous forces. However, as seen in table 1, the present experimental results do not support this conclusion. In fact, it is obvious that the liquid drop breakup regimes scale with the Weber number instead, and not with the Reynolds number. For example, cases 1 and 8 have similar Reynolds numbers (863 and 1097, respectively, i.e. to within 21%) but, as seen in figures 4 and 10 they lie in completely different breakup regimes (i.e. in the bag and so-called shear regimes, respectively). Or, from table 1 it is seen that in case 5 the Weber number and the Reynolds number are 260 and 1458, respectively, and in case 9 the Weber number and the Reynolds number are 463 and 1464, respectively. Although the Reynolds numbers are almost same in the two cases, the drop breakup regimes are again quite different. Case 5 is in the so-called shear breakup regime, while case 9 is in the 'catastrophic' regime (see below). A comparison of case 2 with case 6 in table 1, gives the same conclusion. On the other hand, cases 2, 5 and 8 in table 1 (see also figures 5, 9 and 10) which all have the same Weber number (260), but whose Reynolds numbers are 1866, 1458 and 1097, respectively, all belong to the same regime (i.e. breakup with the sheet thinning and deflection mechanism described above).

Figures 9 and 10 show the experimental results of the breakup of the smaller drops with a Weber number of 260. In figure 9, the original drop size is 121 μm, and the air velocity is 188 m/s. In figure

10, the original drop size is 69 μm, and the air velocity is 248 m/s. From inspection of figures 5, 9 and 10, it can be seen that all of them belong in the same drop-edge sheet-thinning and deflection regime.

From the above analyses, it is concluded that the occurrence of drop breakup in this regime depends primarily on the value of the drop Weber number. The Weber number is the ratio of inertia to surface tension forces, and it also dominates over viscous effects (Reynolds number effects) in the deformation and thinning process of the drop (see below and [5]). Once again, it is important to note that the present experimental results cast considerable doubt on the validity of the so-called shear or boundary-layer stripping breakup mechanisms. Also note that the present proposed sheet-thinning and deflection mechanism applies even in inviscid liquid and gas flows, and this is consistent with the fact that the Reynolds number is seen in the present experiments not to influence the breakup mechanism appreciably.

5.2.3. Catastrophic breakup. As the air velocity is further increased, the so-called 'catastrophic' breakup phenomenon occurs. Figure 6 shows the catastrophic breakup process in which the original drop size is 198 μm, and the air velocity is 196 m/s, with a corresponding Weber number of 463. From a comparison of figure 6 with figure 5, it is obvious that they have some similarities; that is, in the catastrophic regime the drop is also flattened significantly, with its convex surface facing toward the flow of air. The edges of the saucer-shaped body are drawn out into a thin sheet by the suction stress at the equator of the flattened drop due to the high-speed air flow. The sheet is then split up into fine filaments or ligaments which break up into small drops.

The similar breakup phenomena seen in figures 6 and 5 for drops in the so-called shear and 'catastrophic' breakup regimes suggest that they have analogous breakup mechanisms. For example, (1) the sheet edge of the flattened drop is bent in the direction of the flow of air by the air stream blowing, which makes the flattened drop exhibit a convex surface facing the air flow, (2) the production of folds on the thin edge sheet in the azimuthal direction caused by the bending of the sheet edge leads to the production of filaments.

However further comparison of figure 6 with figure 5 reveals that they also have some different breakup features. For example, in figure 6 the growth of unstable surface waves can be observed on the windward flattened drop surfaces in the azimuthal direction. These surface waves are likely to be capillary waves, as suggested by Hinze (1955) and others, because in high relative velocity fields the surface tension forces play a dominant role in the drop deformation and disintegration process, and the effect of gravity is negligible. However, as noted by Hwang *et al.* (1996), these waves could possibly be due to Rayleigh–Taylor instabilities promoted by the large acceleration of the drop as it enters the air stream. In a study of drop breakup in high intensity sound fields, photographs of the top side surface of flattened drops also exhibited evidence of capillary waves on the flattened drop surfaces in the azimuthal direction (Lee *et al.* 1991), which could be similar to the waves seen in the present experimental results.

Large scale unstable surface waves can significantly increase the production of filaments. Furthermore, due to their unstable growth, these surface waves can tear the flattened drops into large fragments, as noted by Hwang *et al.* (1996). Therefore it is believed that at high relative velocities the growth of surface waves on the flattened drop surfaces in the azimuthal direction combined with the bending and folding of the flattened sheet edge makes the breakup processes demonstrate 'catastrophic' breakup characteristics.

Figures 11 and 12 show the experimental results of the breakup of the smaller drops with the highest Weber number of the study, 463. In figure 11, the original drop size is 121 μm, and the air velocity is 250 m/s. In figure 12, the original drop size is 69 μm, and the air velocity is 331 m/s. From inspection of figures 6, 11 and 12, it can be seen that all of them illustrate the typical 'catastrophic' breakup features.

In summary, the experimental results shown in Figures 4–12 confirm that the breakup regimes depend primarily on the value of the Weber number in all three regimes. For example, in cases 3, 6 and 9 the Weber numbers are 463; the Reynolds numbers are 2488, 1939 and 1464, respectively. Although there is a large difference between the Reynolds numbers, the three cases are in the same 'catastrophic' breakup regime, since the Weber number values are same in the three cases.

5.3. *Model predictions*

The preceding discussions highlight the importance of the distortion of the drops on the breakup process in all three breakup regimes. This distortion was seen to be an integral part of the breakup process also in the so-called shear or boundary-layer stripping and in the 'catastrophic' regimes. The importance of the distortion effect was not considered in previously proposed hypothetical breakup mechanisms in those regimes. The trajectory of a drop is also highly influenced by its distortion due to the effect of distortion on drop drag. Thus, a study of drop trajectories is useful to provide further supporting evidence of the fundamental role of drop distortion in the breakup process.

Figures 13–15 show predictions using [6] of the first breakup stage of the breakup process in which the liquid drops are accelerated by the air flow as they enter the air jet. The distortion processes of the liquid drops is predicted by using the DDB model for the different size drops under the various air velocity conditions. Figure 13(a), (b) and (c) illustrate the drop trajectory and deformation processes at 10 μs intervals for the case where the injected drop diameter is 198 μm in the bag (air velocity 68 m/s, Weber number 56), the shear (air velocity 147 m/s, Weber number 260) and the catastrophic (air velocity 196 m/s, Weber number 463) breakup regimes, respectively. Figure 14(a), (b) and (c) show the drop deformation processes at 5 μs intervals for the drop diameter of 121 μm in the bag (air velocity 87 m/s, Weber number 56), the shear (air velocity

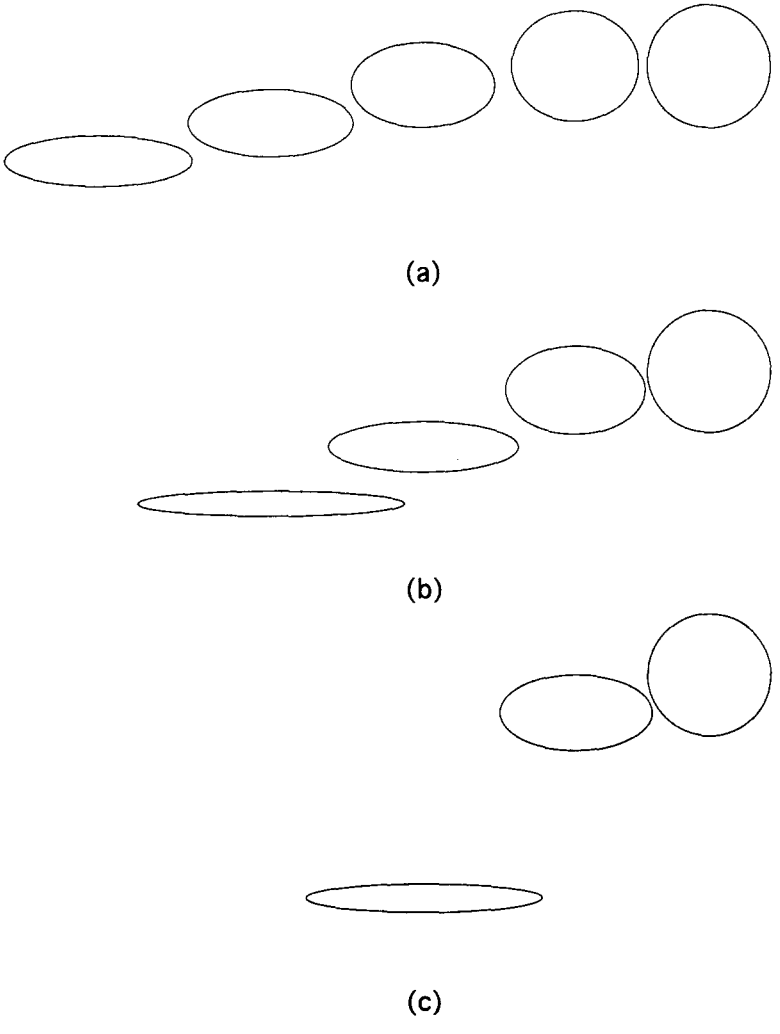

Figure 13. Predicted drop trajectory and distortion for 198 μm drop diameter at 10 μs intervals under action of air velocity of (a) 68 m/s, We = 56, (b) 147 m/s, We = 260, and (c) 196 m/s, We = 463.

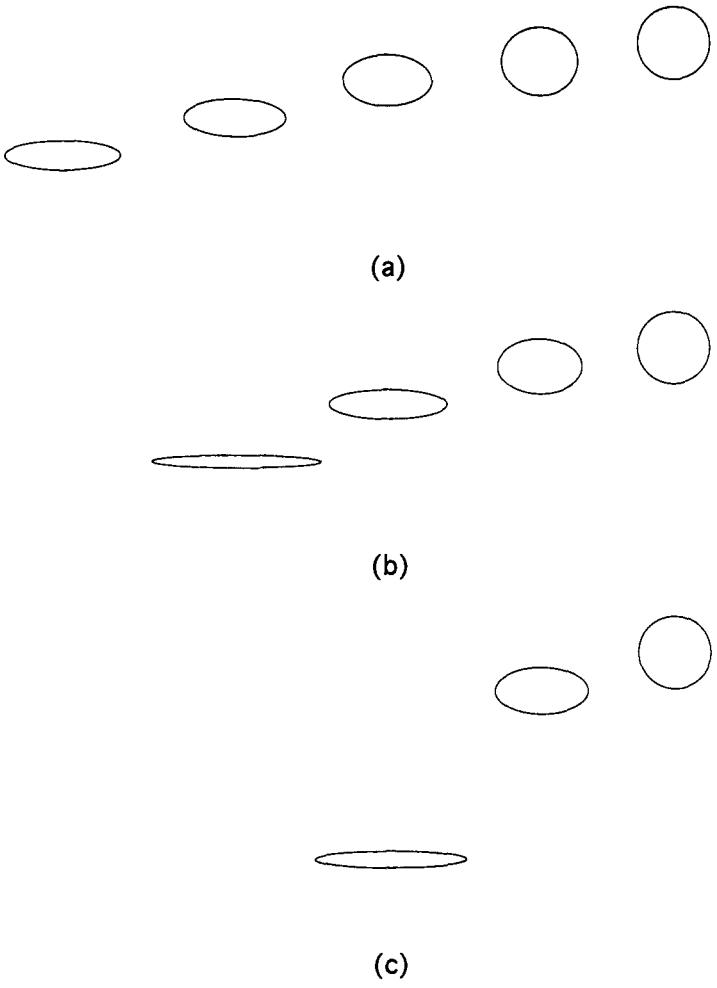

Figure 14. Predicted drop trajectory and distortion for 121 μm drop diameter at 5 μs intervals under action of air velocity of (a) 87 m/s, We = 56, (b) 188 m/s, We = 260, and (c) 250 m/s, We = 463.

188 m/s, Weber number 260) and the catastrophic (air, velocity 250 m/s, Weber number 463) breakup regimes, respectively. Finally, figure 15(a), (b) and (c) illustrate the drop deformation processes at 2 μs intervals with the drop diameter of 69 μm in the bag (air velocity 115 m/s, Weber number 56), the shear (air velocity 248 m/s, Weber number 260) and the catastrophic (air velocity 331 m/s, Weber number 463) breakup regimes, respectively.

From inspection of figures 13–15, it is obvious that (1) when the air velocity is increased, the rate of the drop deformation process increases correspondingly; and (2) when the drop size is reduced, the rate of the drop deformation also increases subsequently. Therefore, both the air velocity and the initial drop size have significant effects on the drop deformation process. When the air velocity is high and the initial drop size is small, the time period needed for drop to become fully distorted is short.

Figures 16–18 show comparisons of the distortion process of liquid drops predicted by using DDB model together with the present experimental results. X is the drop's horizontal displacement (see figure 1), and a is the drop's major semiaxis. The initial drop diameter is 198 μm in figure 16, 121 μm in figure 17 and 69 μm in figure 18. From figures 16–18 it is evident that the results calculated by using the DDB model are in reasonably good agreement with the measured data for drops in each of the bag, so-called shear, and 'catastrophic' breakup regimes. However, the predicted drop distortion underestimates the measured data somewhat as time progresses because the present model does not account for the deflection of the thinned edge of high speed drops by the air flow.

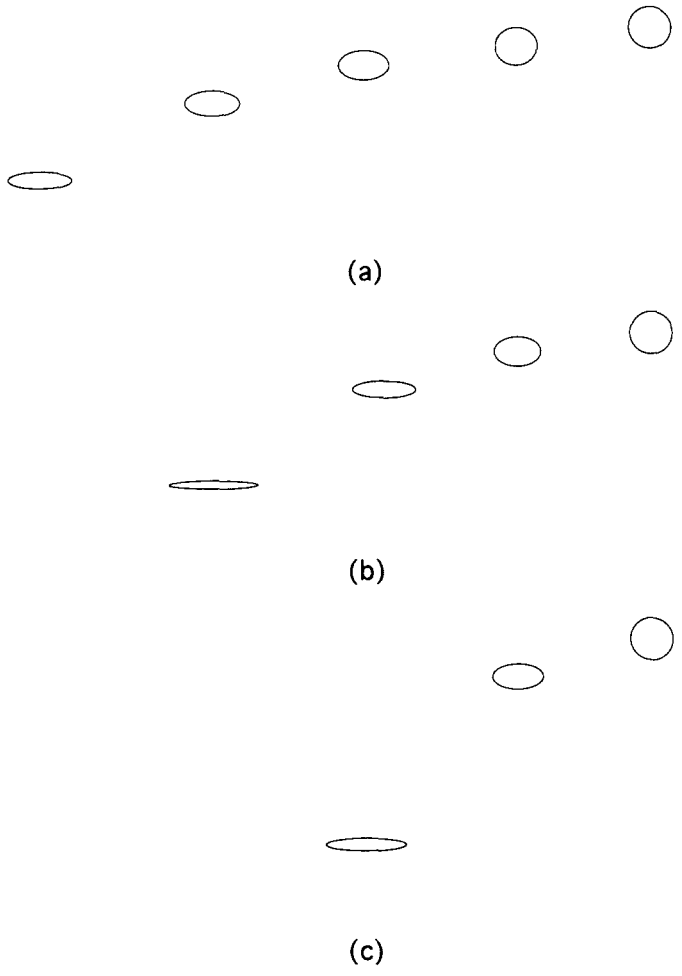

Figure 15. Predicted drop trajectory and distortion for 69 μm drop diameter at 2 μs intervals under action of air velocity of (a) 115 m/s, We = 56, (b) 248 m/s, We = 260, and (c) 331 m/s, We = 463.

The trajectory of the drops during their interaction with the air jet provides additional information about the drag coefficients of the drops during the flattening process. Figures 19–21 show the model predictions of the drop trajectories together with the experimental data for the

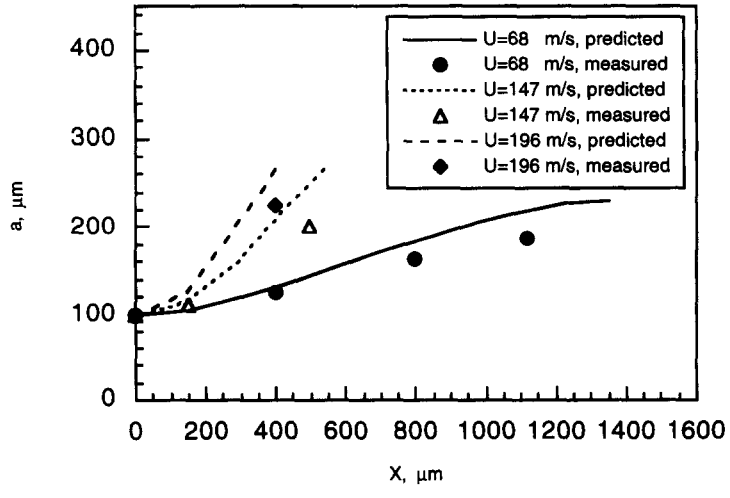

Figure 16. Model prediction of drop distortion for 198 μm drop with experimental data.

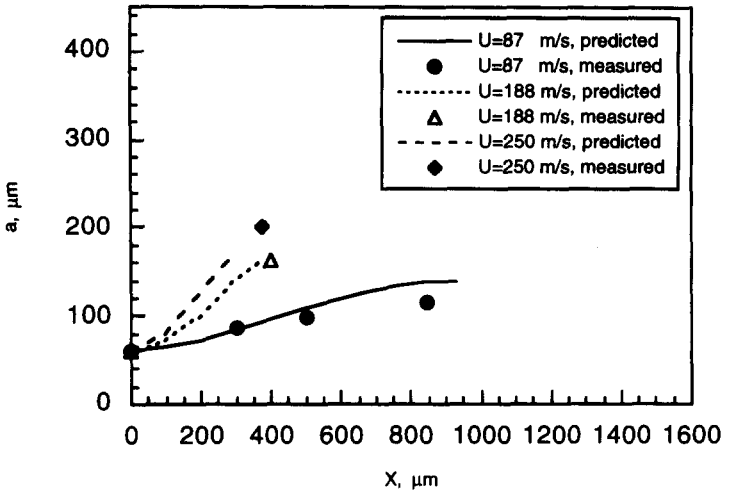

Figure 17. Model prediction of drop distortion for 121 μm drop with experimental data.

different drop sizes in the three breakup regimes. In these three figures X is the horizontal displacement of drop, and Y is the vertical displacement of drop. For the purpose of the present study the trajectories were defined by tracking the location of the furthest (horizontal) penetrating boundary of the distorting drop.

Figure 19 shows the trajectory of drop with an initial diameter of 198 μm, figure 20 shows the trajectory of drop with an initial diameter of 121 μm, and figure 21 shows the trajectory of drop with an initial diameter of 69 μm. The predicted and measured trajectories agree reasonably with in all cases. It can be seen that there is a common feature in these three figures, that is, the drop trajectories become steeper as the air-jet velocity is increased. From further inspection of figures 19–21, it can be seen that the drop trajectories also become steeper as the initial drop diameter is reduced in the same breakup regime (same initial Weber number).

In these figures the experimental results strongly support the present drop distortion and trajectory predictions. However it should be noted that since the distortion and trajectory of liquid drops are computed dynamically without modeling the subsequent breakup of the drops, the predictions are strictly only valid during the first stage of the breakup process. The present drop distortion and trajectory comparisons also show that the distortion depends primary on the drop Weber number; analysis of the results shows that the term containing viscous effects in [6] makes

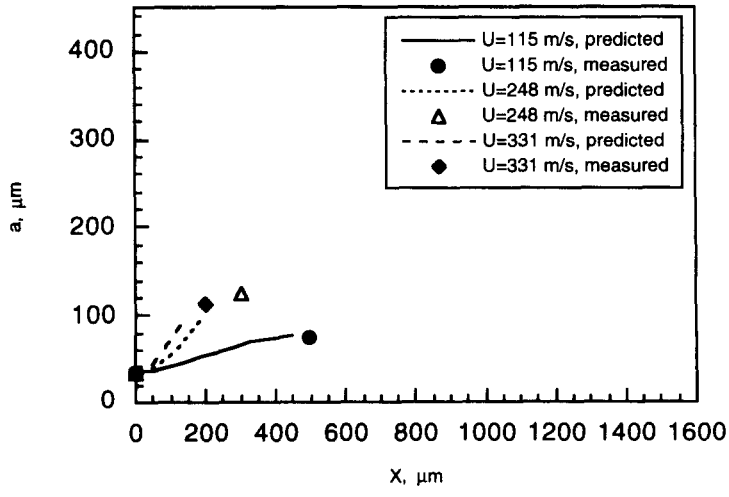

Figure 18. Model prediction of drop distortion for 69 μm drop with experimental data.

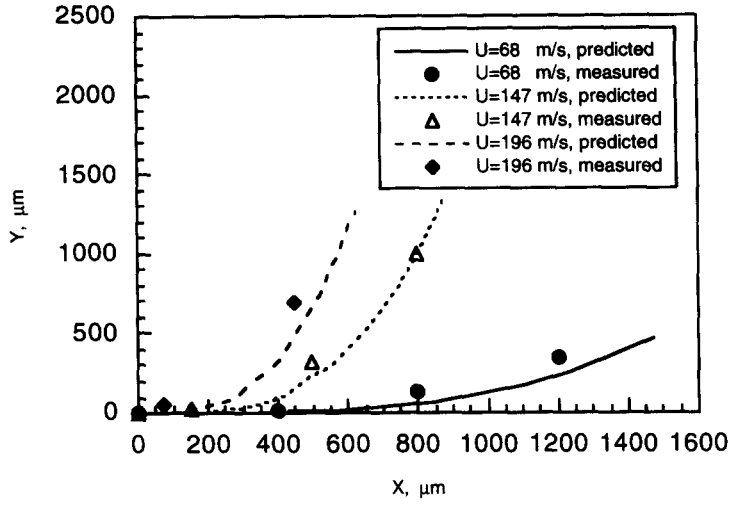

Figure 19. Model prediction of trajectory for 198 μm drop with experimental data.

only a small contribution to the drop distortion. Again, this confirms the results of the previous section which show the dominant effect of the Weber number on the breakup process.

6. CONCLUSIONS

Experiments and model predictions have been performed by using different size drops exposed to high speed air flows to investigate the distortion and breakup mechanisms of liquid drops. Based on the information presented by the experimental and calculated results and the analyses above, the following conclusions were reached.

(1) The breakup process of liquid drops can be classified roughly into two stages. During the first stage of the drop breakup process, the drops experience a shape change. Under the action of aerodynamic pressure the drops become distorted from their undisturbed spherical shapes and become flattened, or disk shaped, normal to the air flow direction. All three drop breakup regimes exhibit this common feature. During the second stage of the drop breakup process, the distorted drops undergo a disintegration, and the three drop breakup regimes display different breakup mechanisms.

(2) During the second stage of the bag breakup regime, the appearance and growth of holes on the bag sheet which is blown out from the center of the flattened drop is the dominant reason for the production of filaments which are stretched out and are aligned with the air flow direction.

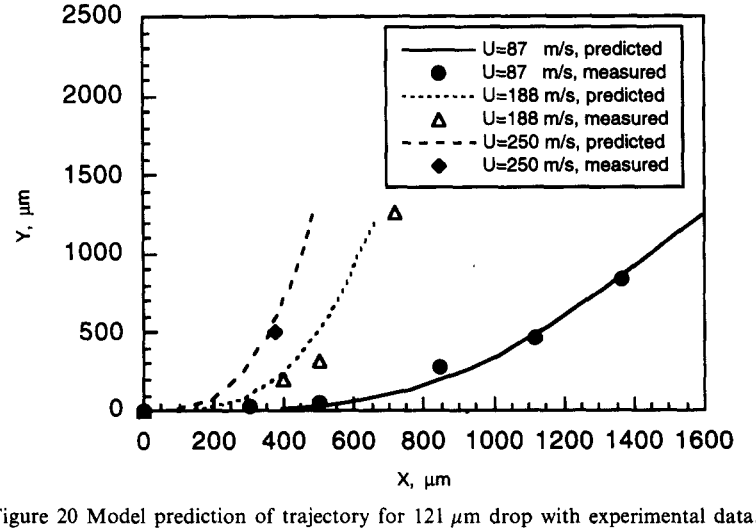

Figure 20 Model prediction of trajectory for 121 μm drop with experimental data.

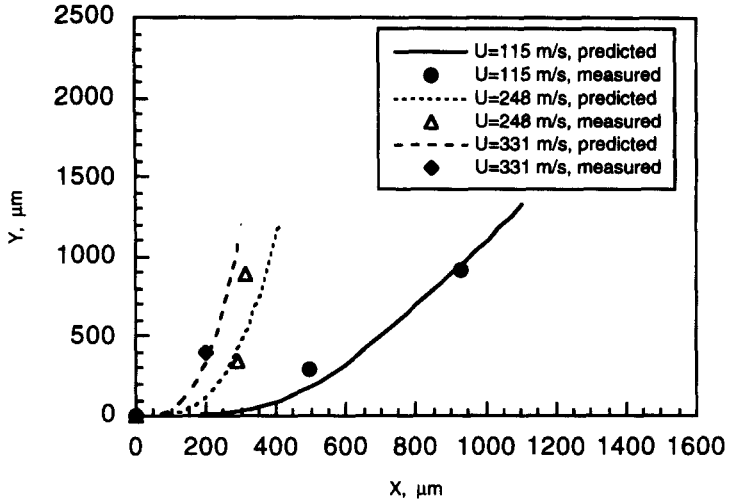

Figure 21. Model prediction of trajectory for 69 μm drop with experimental data.

(3) During the second stage of the so-called shear or boundary layer stripping breakup regime, the bending of the thinned sheet formed at the equatorial edges of the flattened drop under the action of air blowing, followed by the production of folds on the bending sheet results in production of ligaments that are aligned in the direction of air flow. These ligaments subsequently breakup into droplets. This is a qualitatively different breakup mechanism than that of previously proposed mechanisms which ascribe the breakup to viscous shear or boundary layer stripping mechanisms. The present proposed sheet-thinning and deformation breakup mechanism applies even in inviscid flows, and this explains why the Weber number is the dominant parameter in the breakup process. The present results imply that the term 'shear breakup' does not adequately represent the physical mechanism of breakup in the so-called shear or boundary-layer stripping regime. A suggested improved term is breakup in the 'sheet thinning and deformation' regime.

(4) During the second stage of the 'catastrophic' breakup regime, the unstable growth of capillary (possibly Rayleigh–Taylor) waves on the flattened drop surfaces, combined with bending and folding of the thinned liquid sheet at the equatorial edges of the flattened drop makes the breakup processes demonstrate 'catastrophic' breakup characteristics.

(5) The experimental results under the various parameter conditions considered confirm that breakup in all three breakup regimes depends primarily on the Weber number and not on the Reynolds number. The Reynolds number would be expected to important if the breakup process was controlled by shear forces, as has previously been proposed.

(6) The distortion of a drop prior to its breakup is controlled by the drop Weber number and the drop's distortion has a significant effect on its drag coefficient. A dynamic drag model that accounts for the increase of both the drop's frontal area and its drag coefficient as a function of its distortion was used to help quantify the distortion process. The model predictions of drop trajectories and drop distortions during the first stage of the drop breakup process and the experimental results are in good agreement for the different size drops in the three breakup regimes. These results also support the conclusion that drop distortion and aerodynamic thinning forms an integral part of the breakup process for high speed drops.

Acknowledgements—Support was provided by Caterpillar Inc. and the U.S. Army Research Office.

REFERENCES

Anilkumar, A. V., Lee, C. P. and Wang, T. G. (1993) Stability of an acoustically levitated and flattened drop: an experimental study. *Physics of Fluids* **A5**, 2763–2774.

Berglund, R. N. and Liu, Y. H. (1973) Generation of monodisperse aerosol standards. *Experimental Science & Technology* **7**, 147–153.

Chigier, N. A. and Reitz, R. D. (1996) Regimes of jet breakup and breakup mechanisms. In *Progress in Astronautics and Aeronautics*, ed. K. Kuo, Vol. I, pp. 109–136.

Collins, R. and Charwat, A. F. (1971) The deformation and mass loss of liquid drops in a high speed flow of gas. *Israel J. Tech.* **9,** 43–54.

Danilov, S. D. and Mironov, M. A. (1992) Breakup of a droplet in a high-intensity sound field. *J. Acoust. Soc. Am.* **92,** 2747–2755.

Engel, O. G. (1958) Fragmentation of waterdrops in the zone behind an air shock. *Journal of Research of the National Bureau of Standards* **60,** 245–280.

Hinze, J. O. (1955) Fundamentals of the hydrodynamic mechanism of splitting in dispersion processes. *American Institute of Chemical Engineering Journal* **1,** 289–295.

Hsiang, L. P. and Faeth, G. M. (1992) Near limit drop deformation and secondary breakup. *Int. J. Multiphase Flow* **19,** 635–652.

Hwang, S. S., Liu, Z. and Reitz, R. D. (1996) Breakup mechanisms and drag coefficients of high speed vaporizing liquid drops. *Atomization and Sprays* **6,** 353–376.

Ibrahim, E. A., Yang, H. Q. and Przekwas, A. J. (1993) Modeling of spray droplets deformation and breakup. *AIAA J. Propulsion and Power* **9,** 651–654.

Kennedy, J. B. and Roberts, J. (1990) Rain ingestion in a gas turbine engine. *Proceedings of 4th ILASS Meeting*, Hartford, CT, p. 154.

Krzeckowski, S. A. (1980) Measurement of liquid droplet disintegration mechanism. *Int. J. Multiphase Flow* **6,** 227–239.

Lee, C. P., Anilkumar and Wang, T. G. (1991) Static shape and instability of an acoustically levitated liquid drop. *Phys. Fluids* **A3,** 2497–2515.

Lefebvre, A. H. (1989) *Atomization and Sprays*. Hemisphere Publications, New York.

Liu, A. B., Mather, D. and Reitz, R. D. (1993) Effects of drop drag and breakup on fuel sprays. SAE paper 930072.

Liu, A. B. and Reitz, R. D. (1993) Mechanism of air assisted liquid atomization. *Atomization and Spray* **3,** 55–75.

O'Rourke, P. J. and Amsden, A. A. (1987) The TAB method for numerical calculation of spray droplet breakup. SAE paper 872089.

Pilch, M. and Erdman, C. A. (1987) Use of breakup time data and velocity history data to predict the maximum size of stable fragments for acceleration—induced breakup of liquid drop. *Int. J. Multiphase Flow* **13,** 741–757.

Ranger, A. A. and Nicholls, J. A. (1969) The aerodynamic shattering of liquid drops. *AIAA J.* **7,** 285–290.

Reinecke, W. G. and Waldman, G. D. (1970) A study of drop breakup behind strong shocks with applications to flight. *AVCO Report AVSD-0110-70-77.*

Reitz, R. D. and Bracco, F. V. (1986) Mechanism of breakup of round liquid jets. In *Encyclopedia of Fluid Mechanics*, p. 233. Gulf Pub, Houston, TX.

Spielbauer, T. M. and Aidum, C. K. (1994) The cause and effects of perforation in a liquid sheet from a splash-plate spray nozzle. *Atomization and Sprays* **4,** 405–463.

Squire, H. B. (1953) Investigation of the instability of a moving liquid film. *Brit. J. Appl. Phys.* **4,** 167–169.

Stapper B. E. and Samuelsen, G. S. (1990) An experimental study of the breakup of a two-dimensional liquid sheet in the presence of co-flow air shear. American Institute of Aeronautics and Astronautics, paper AIAA-90-0461, 28th Aerospace Science Meeting, 8–11 January, Reno, NV.

Taylor, G. I. (1959) The dynamics of thin sheets of fluid—III. Disintegration of fluid sheets. *Proc. R. Soc. Lond. A* **253,** 313–321.

Wierzba, A. and Takayama, K. (1988) Experimental investigation of the aerodynamic breakup of liquid drops. *AIAA J.* **26,** 1329.

Wu, P. K. and Faeth, G. M. (1993) Aerodynamic effects primary breakup of turbulent liquids. *Atomization and Sprays* **3,** 265–289.

Wu, P.-K., Hsiang, L.-P. and Faeth, G. M. (1993) Aerodynamic effects on primary and secondary spray breakup. *First International Symposium on Liquid Rocket Combustion Instability.* Pennsylvania State University, PA.